

Effects of weak intramolecular interactions and distortions from trigonal prismatic coordination on the magnetic properties of zero-field Co(II) single-ion magnets

Ben Zhang,^a Yang Zhou,^a Hao-Yi Huang,^a Xiao-Le Zhang,^b Yi Xiang,^a Yanbo Shi,^a Chennan Zhang,^a Aihua Yuan,^a Xingwei Cai,^a Lei Chen,^{*a} Yi-Quan Zhang,^{*b} and Zhao-Bo Hu^{*c}

^aSchool of Environmental and Chemical Engineering, Jiangsu University of Science and Technology, Zhenjiang 212003, PR China.

^bJiangsu Key Laboratory for NSLSCS, School of Physical Science and Technology, Nanjing Normal University, Nanjing 210023, PR China.

^cChaotic Matter Science Research Center, Department of Materials, Metallurgy and Chemistry, Jiangxi University of Science and Technology, Ganzhou 341000, PR China.

Electronic Supplementary Information

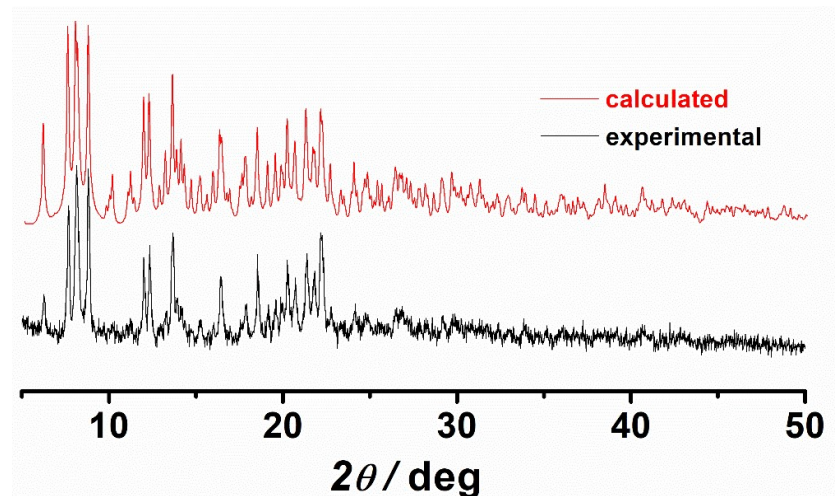


Figure S1. PXRD pattern for **1**-BPh₄.

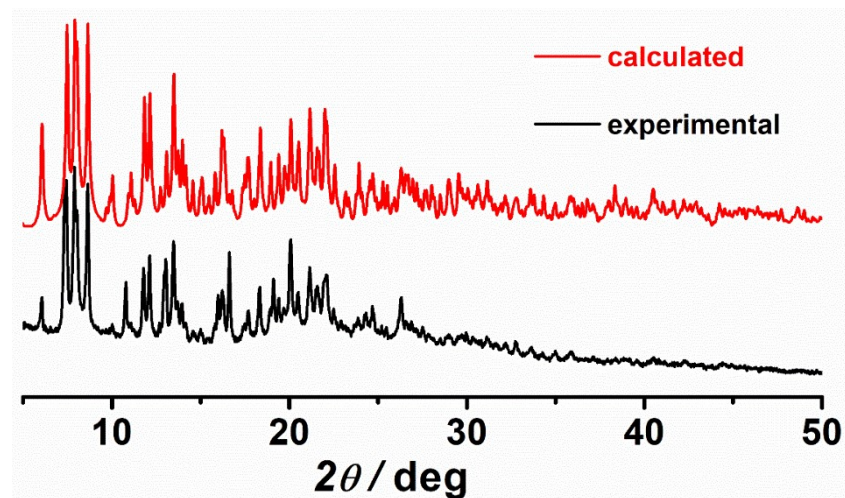


Figure S2. PXRD pattern for **1**-BPh₄@Zn.

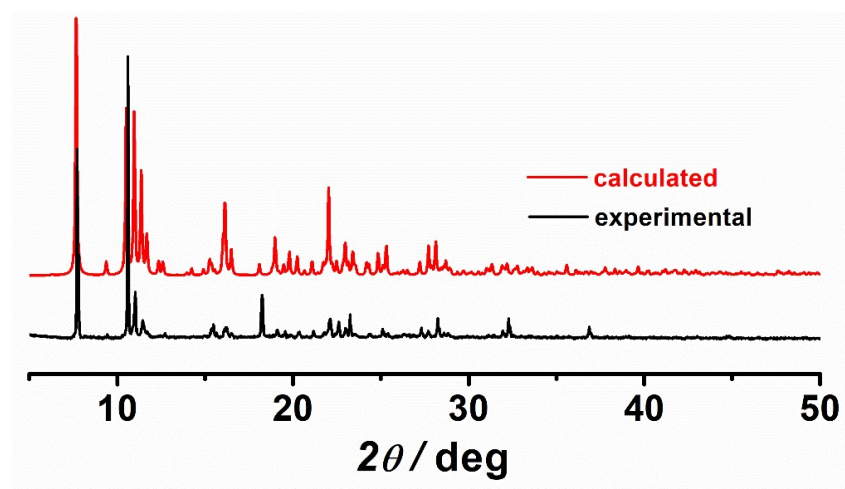


Figure S3. PXRD pattern for **2**-NO₃.

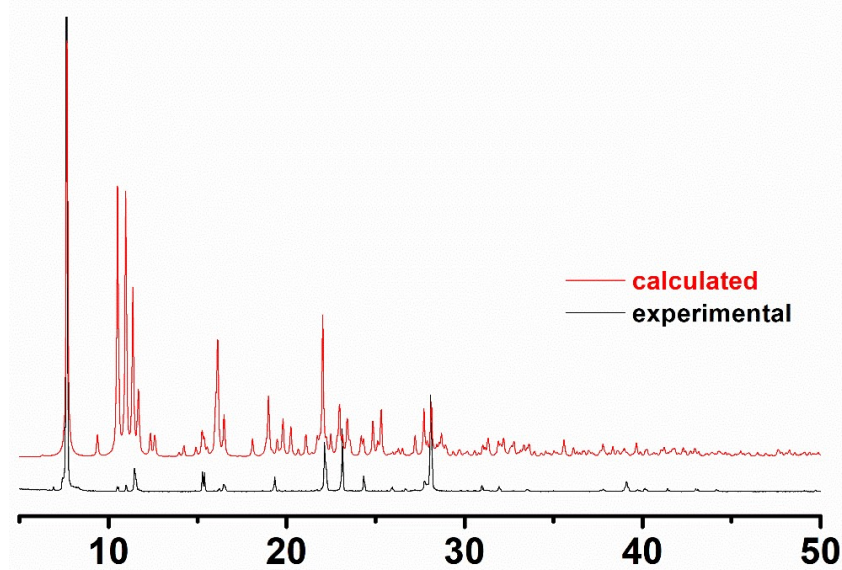


Figure S4. PXRD pattern for **2-NO₃@Zn**.

Table S1. Crystal data and structure refinement for complexes **1-BPh₄**, **Zn-BPh₄** and **2-NO₃**.

| | 1-BPh₄ | Zn-BPh₄ | 2-NO₃ |
|--|---|---|--|
| Molecular formula | C ₈₄ H ₉₀ B ₂ CoN ₈ O | C ₈₄ H ₉₀ B ₂ ZnN ₈ O | C ₃₄ H ₄₃ CoN ₁₁ O ₆ |
| CCDC no | 2302669 | 2325454 | 2302668 |
| Formula weight | 1308.18 | 1314.62 | 760.72 |
| Temperature / K | 296(2) | 293(2) K | 296(2) |
| Wavelength / Å | 0.71073 | 1.54178 | 0.71073 |
| crystal system | Triclinic | Triclinic | Triclinic |
| Space group | P-1 | P-1 | P-1 |
| <i>a</i> / Å | 13.4362(10) | 13.4678(4) | 9.4565(13) |
| <i>b</i> / Å | 14.8855(9) | 14.9264(4) | 13.8712(19) |
| <i>c</i> / Å | 18.3909(10) | 18.4215(7) | 14.7616(19) |
| α / deg | 84.615(4) | 84.4150(10) | 72.077(9) |
| β / deg | 83.752(3) | 83.5480(10) | 85.635(9) |
| γ / deg | 78.677(4) | 78.6270(10) | 87.040(9) |
| <i>V</i> / Å ³ | 3575.3(4) | 3596.7(2) | 1836.2(4) |
| <i>Z</i> | 2 | 2 | 2 |
| <i>D</i> _{calc} , g/cm ³ | 1.215 | 1.214 | 1.376 |
| μ / mm ⁻¹ | 0.293 | 0.871 | 0.527 |
| <i>F</i> (000) | 1390 | 1396 | 798 |
| Goodness-of-fit on <i>F</i> ² | 1.029 | 1.134 | 1.025 |
| Final <i>R</i> indices [<i>I</i> > 2σ(<i>I</i>)] ^a | <i>R</i> ₁ = 0.0569, <i>wR</i> ₂ = 0.1389 | <i>R</i> ₁ = 0.0581, <i>wR</i> ₂ = 0.1582 | <i>R</i> ₁ = 0.0382, <i>wR</i> ₂ = 0.0862 |
| <i>R</i> indices (all data) ^a | <i>R</i> ₁ = 0.1107, <i>wR</i> ₂ = 0.1586 | <i>R</i> ₁ = 0.0709, <i>wR</i> ₂ = 0.1715 | <i>R</i> ₁ = 0.0559, <i>wR</i> ₂ = 0.0931 |

^awR₂ = [Σ[w(F_o² - F_c²)²] / Σ[w(F_o²)²]]^{1/2}, R₁ = Σ||F_o|| - |F_c|| / Σ|F_o|.

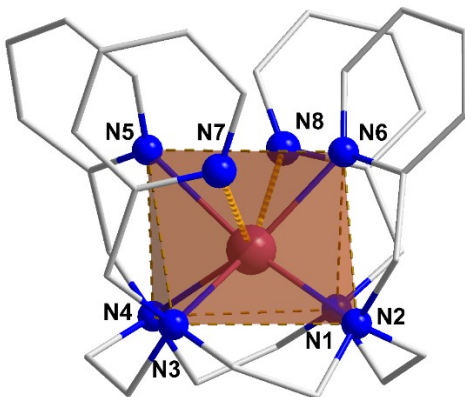


Figure S5. View of the mononuclear complex cation $[\text{Zn}(\text{L}^{\text{N}8})]^{2+}$ in **Zn-BPh₄**. Color scheme: Zn, brown; N, blue; C, gray. Hydrogen atoms are omitted for clarity.

Table S2. Selected bond lengths (\AA) for **1-BPh₄** and **2-NO₃**.

| | 1-BPh₄ | Zn-BPh₄ | | | 2-NO₃ |
|------------|--------------------------|---------------------------|------------|------------|-------------------------|
| Co(1)-N(1) | 2.234(2) | Zn(1)-N(1) | 2.3634(19) | Co(1)-N(1) | 2.2097(17) |
| Co(1)-N(2) | 2.302(2) | Zn(1)-N(2) | 2.301(2) | Co(1)-N(2) | 2.3113(18) |
| Co(1)-N(3) | 2.280(2) | Zn(1)-N(3) | 2.318(2) | Co(1)-N(3) | 2.2002(18) |
| Co(1)-N(4) | 2.313(2) | Zn(1)-N(4) | 2.232(2) | Co(1)-N(4) | 2.3082(18) |
| Co(1)-N(5) | 2.220(2) | Zn(1)-N(5) | 2.2517(18) | Co(1)-N(5) | 2.1490(18) |
| Co(1)-N(6) | 2.139(2) | Zn(1)-N(6) | 2.1349(19) | Co(1)-N(6) | 2.1468(17) |
| Co(1)-N(7) | 3.214(2) | Zn(1)-N(7) | 3.228(2) | Co(1)…N(7) | 5.2476(6) |
| Co(1)-N(8) | 3.177(2) | Zn(1)-N(8) | 3.229(2) | Co(1)…N(8) | 5.2900(6) |

Table S3. Continuous shape measure (CSM) analyses of six-coordinate geometries for **1-BPh₄** and **2-NO₃** by SHAPE software

| Six-coordination | 1-BPh₄ | 2-NO₃ |
|--------------------|--------------------------|-------------------------|
| Hexagon | 34.067 | 34.771 |
| Pentagonal pyramid | 12.992 | 13.221 |
| Octahedron | 10.654 | 11.838 |
| Trigonal prism | 2.451 | 1.575 |

Table S4. Angular parameters α , β , θ , and ϕ of the trigonal prismatic geometry for **1-BPh₄** and **2-NO₃**.

| | 1-BPh₄ | 2-NO₃ | 1-BPh₄ | 2-NO₃ |
|------------|--------------------------|-------------------------|--------------------------|-------------------------|
| α_1 | 95.212° | 93.530° | θ1 | 58.53° |
| α_2 | 77.736° | 79.251° | θ2 | 46.45° |
| α_3 | 75.380° | 76.437° | θ3 | 44.85° |
| α_4 | 94.996° | 93.236° | θ4 | 58.40° |
| α_5 | 78.463° | 79.686° | θ5 | 46.13° |
| α_6 | 74.754° | 76.771° | θ6 | 45.49° |
| β_1 | 92.517° | 87.493° | φ1 | 29.35° |
| β_2 | 77.317° | 77.992° | φ2 | 9.84° |
| β_3 | 76.348° | 77.646° | φ3 | 9.19° |

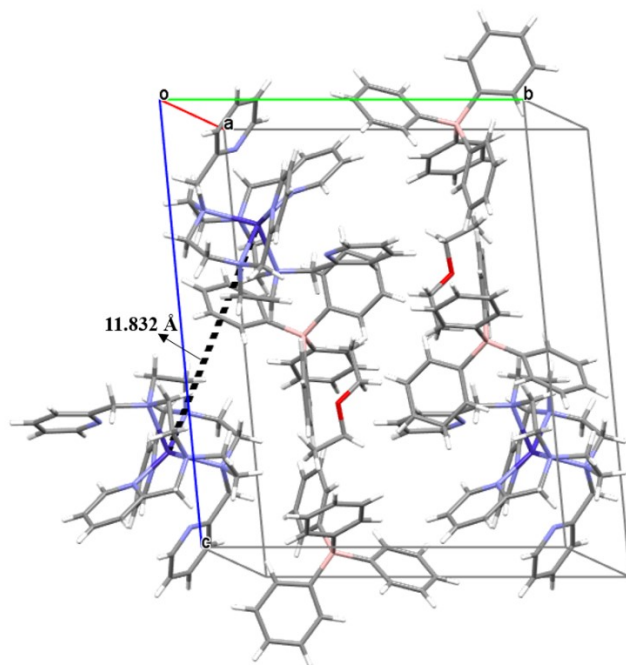


Figure S6. Stacking between adjacent complexes in **1-BPh₄**.

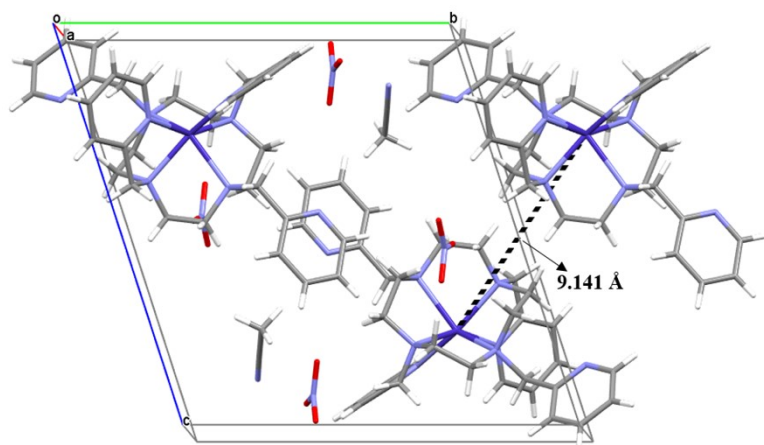


Figure S7. Stacking between adjacent complexes in **2-NO₃**.

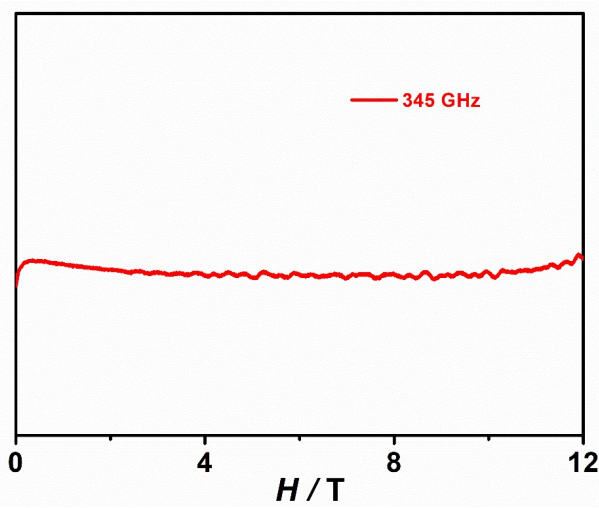


Figure S8. HFEPR spectra for **1-BPh₄** at 2 K.

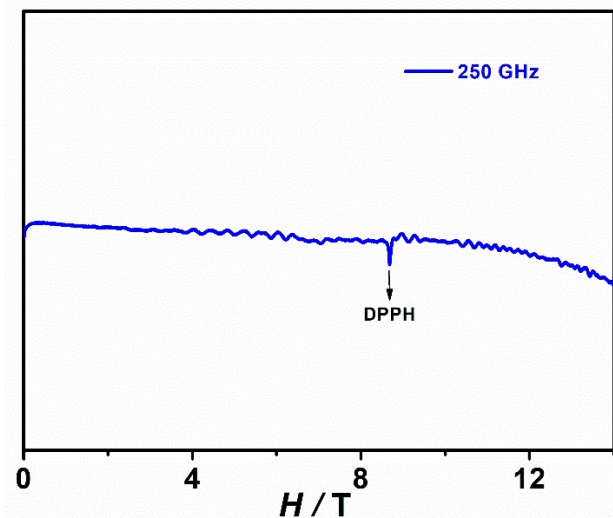


Figure S9. The HFEPR spectra for $\mathbf{2-NO}_3$ at 2 K.

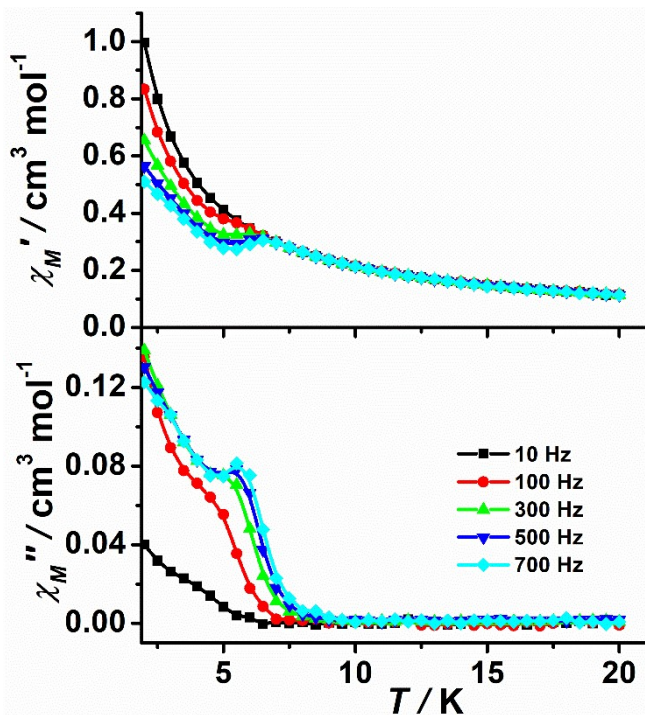


Figure S10. Temperature dependence of in-phase (top) and out-of-phase (bottom) ac susceptibility for $\mathbf{1-BPh}_4$ in zero dc field; solid lines are guides for the eye.

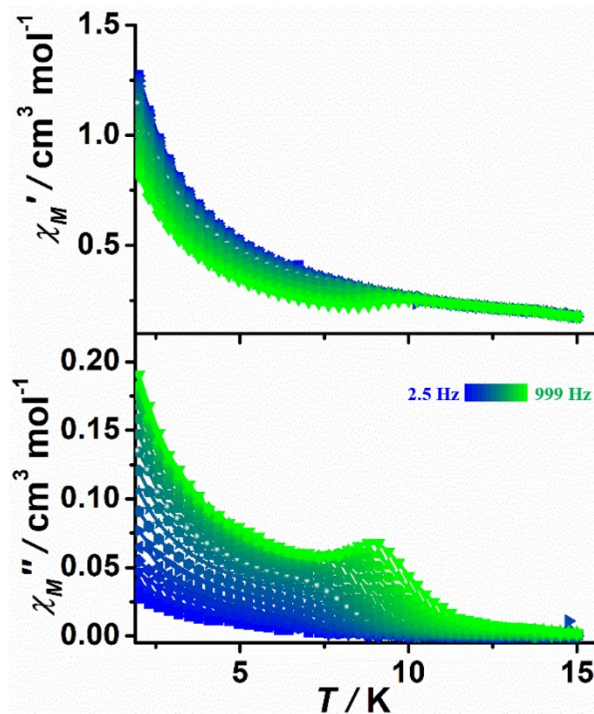


Figure S11. Temperature dependence of in-phase (top) and out-of-phase (bottom) ac susceptibility for **2-NO₃** in zero dc field; solid lines are guides for the eye.

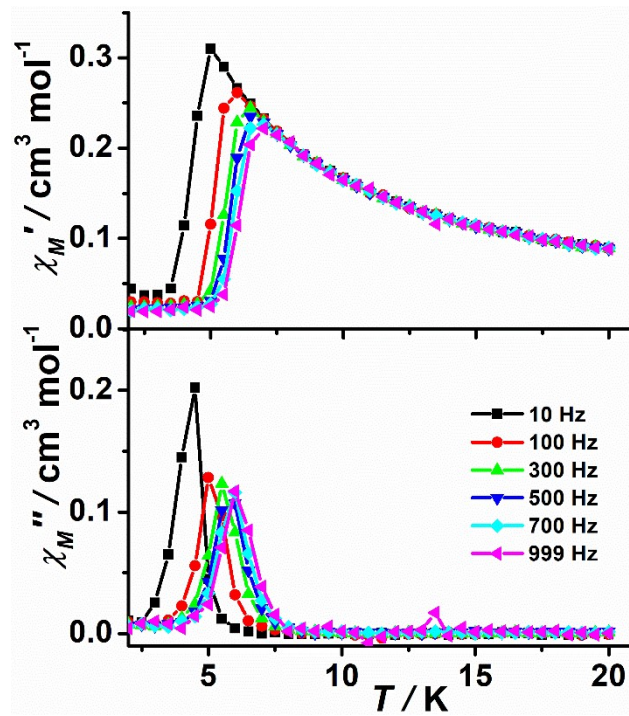


Figure S12. Temperature dependence of in-phase (top) and out-of-phase (bottom) ac susceptibility for **1-BPh₄** in the dc field of 200 Oe; solid lines are guides for the eye.

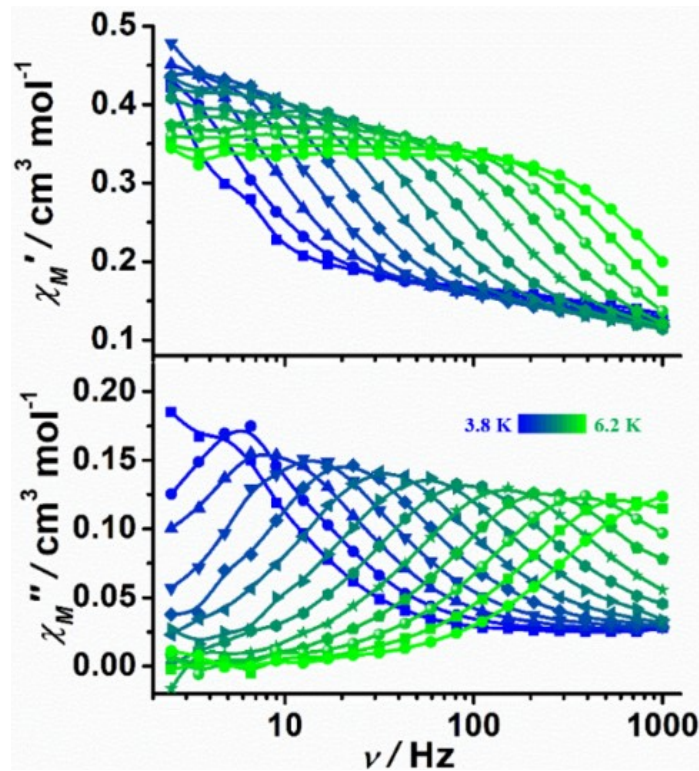


Figure S13. Frequency dependence of in-phase (top) and out-of-phase (bottom) ac susceptibility for **1-BPh₄** in the dc field of 200 Oe; solid lines are guides for the eye.

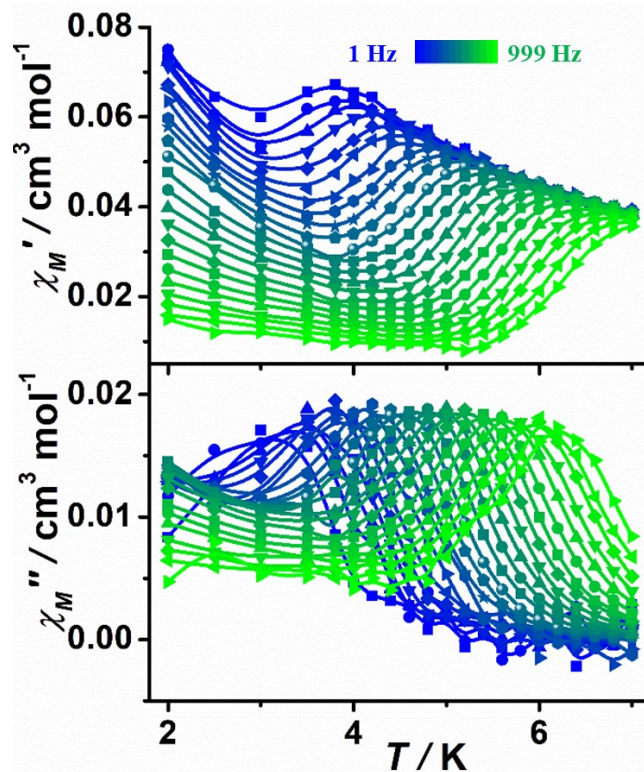


Figure S14. Temperature dependence of in-phase (top) and out-of-phase (bottom) ac susceptibility for **1-BPh₄@Zn** in zero dc field; solid lines are guides for the eye.

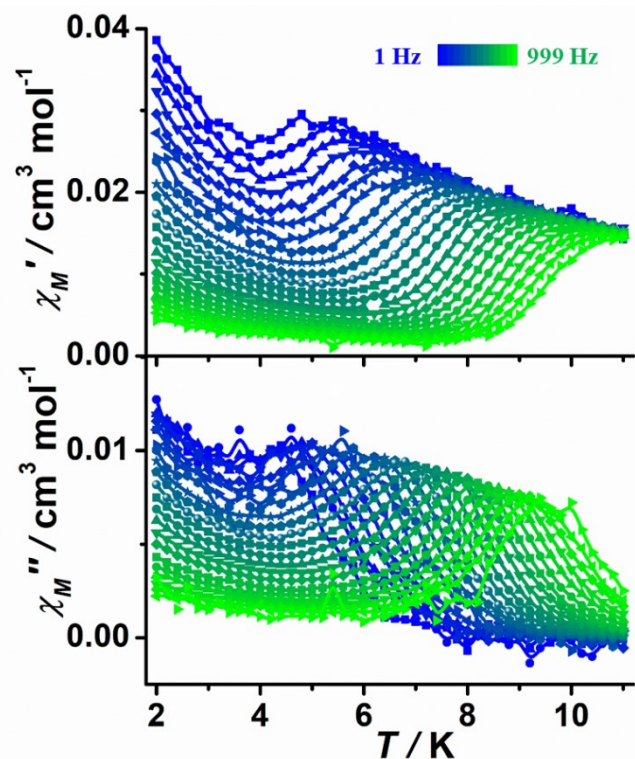


Figure S15. Temperature dependence of in-phase (top) and out-of-phase (bottom) ac susceptibility for **2-NO₃@Zn** in near dc field; solid lines are guides for the eye.

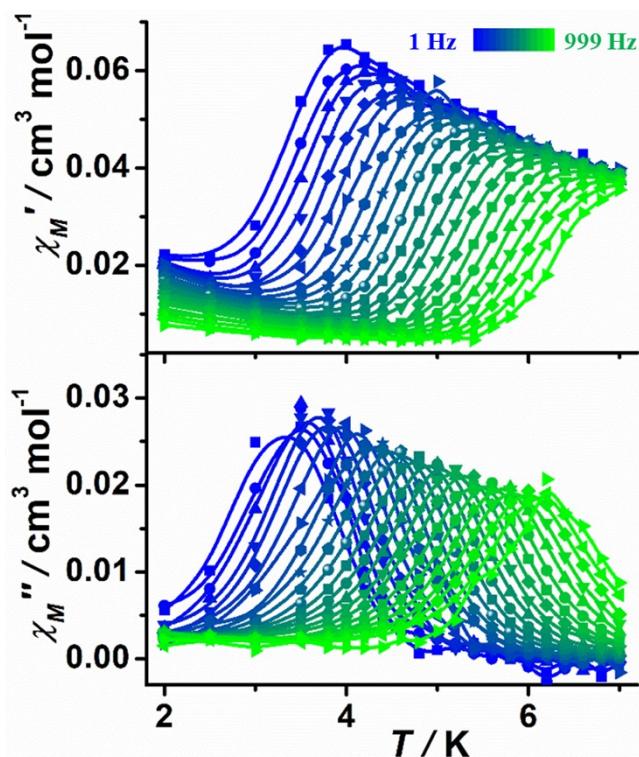


Figure S16. Temperature dependence of in-phase (top) and out-of-phase (bottom) ac susceptibility for **1-BPh₄@Zn** in 200 Oe dc field; solid lines are guides for the eye.

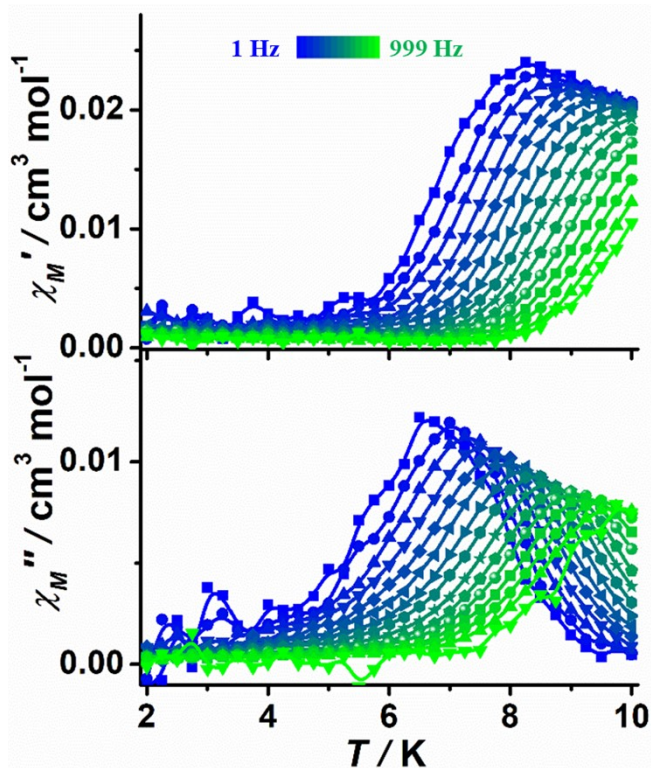


Figure S17. Temperature dependence of in-phase (top) and out-of-phase (bottom) ac susceptibility for **2-NO₃@Zn** in the dc field of 1000 Oe; solid lines are guides for the eye.

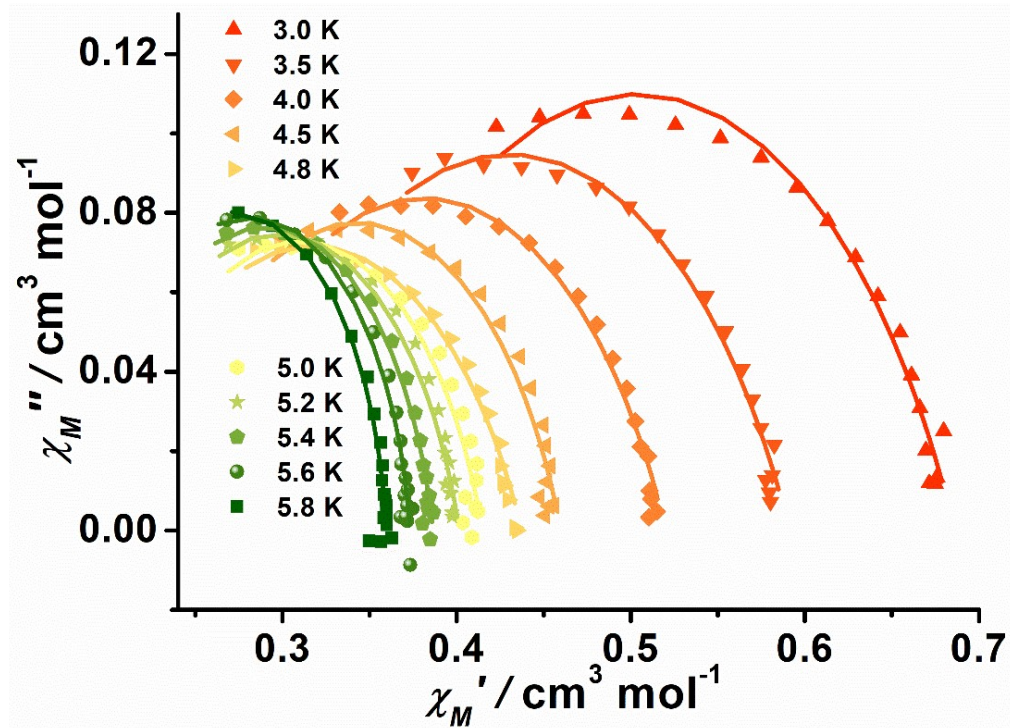


Figure S18. Cole-Cole plots for the ac susceptibilities under zero dc field for **1-BPh₄**. Solid lines represent the best fit for the generalized Debye model.

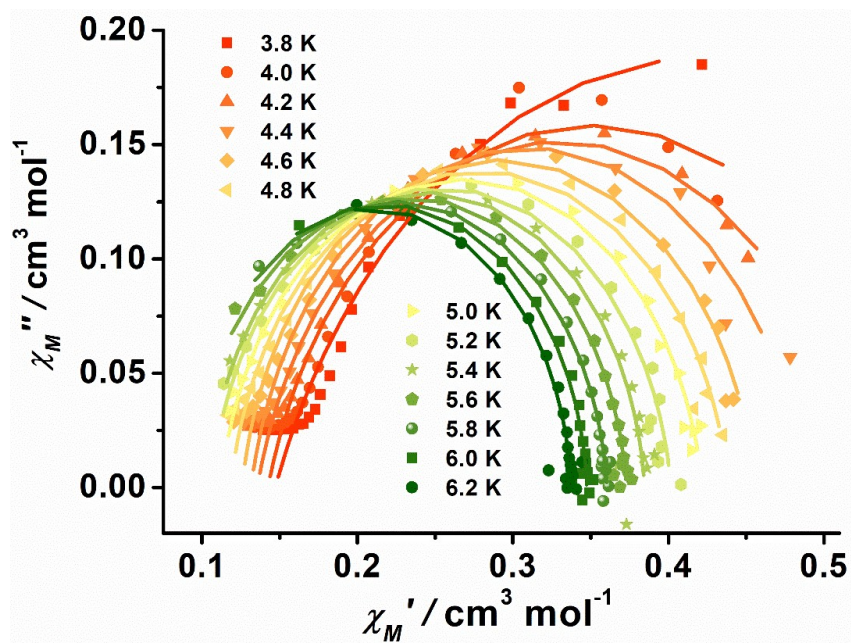


Figure S19. Cole-Cole plots for the ac susceptibilities under 200 Oe dc field for **1-BPh₄**. Solid lines represent the best fit for the generalized Debye model.

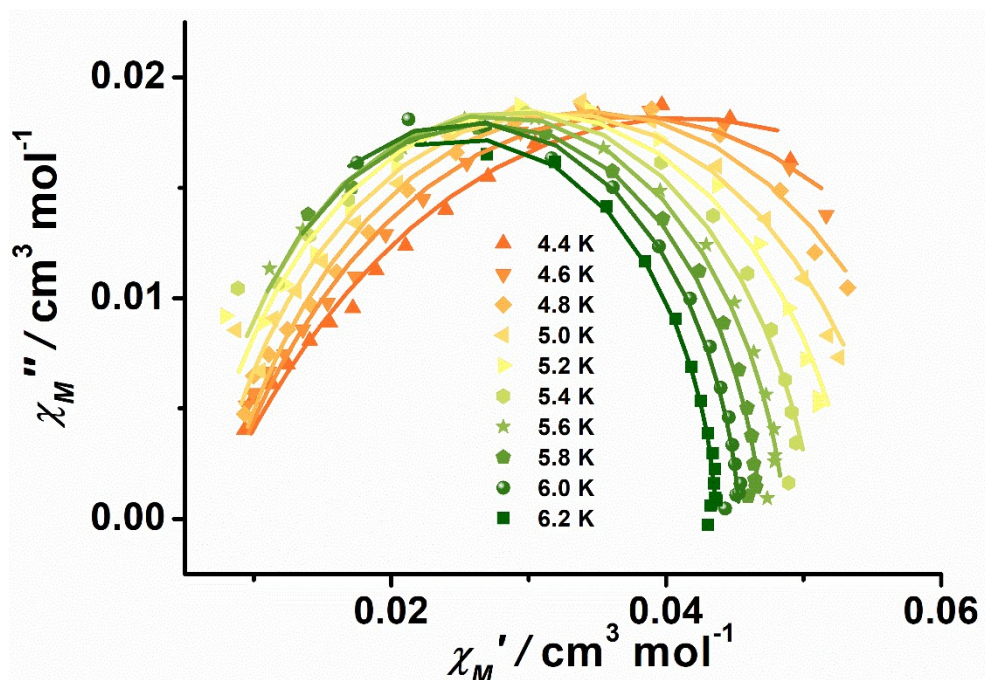


Figure S20. Cole-Cole plots for the ac susceptibilities under zero dc field for **1-BPh₄@Zn**. Solid lines represent the best fit for the generalized Debye model.

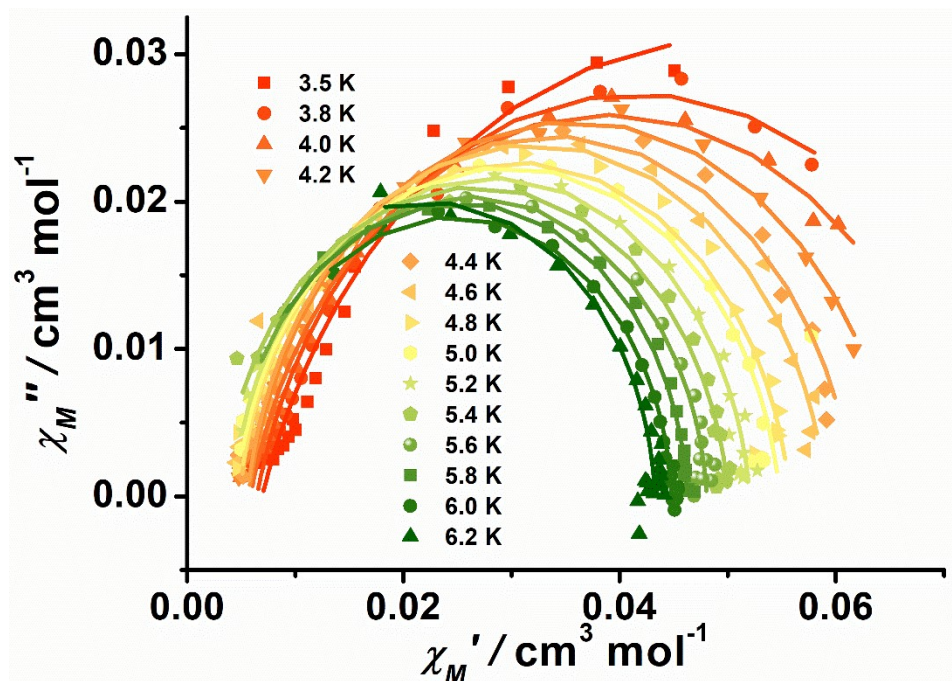


Figure S21. Cole-Cole plots for the ac susceptibilities under 200 Oe dc field for **1-BPh₄@Zn**. Solid lines represent the best fit for the generalized Debye model.

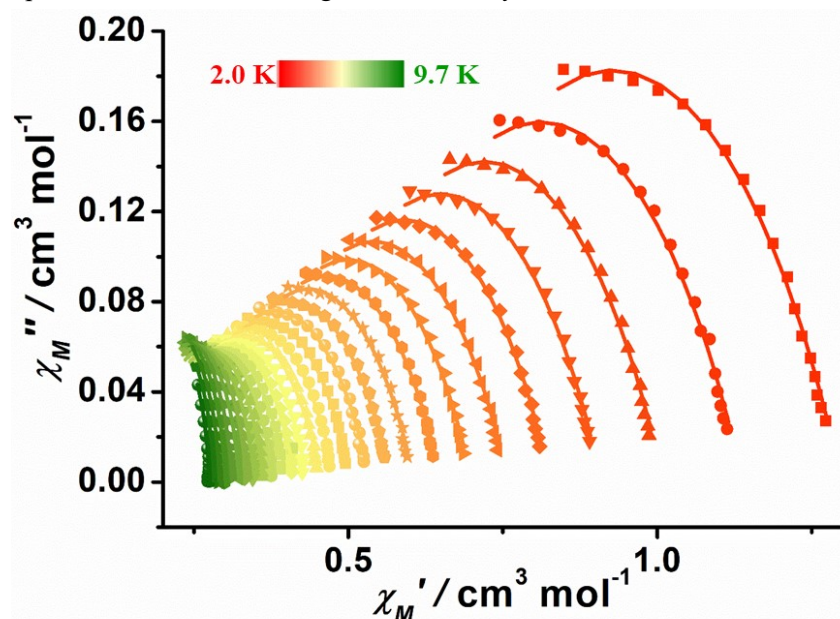


Figure S22. Cole-Cole plots for the ac susceptibilities under zero dc field for **2-NO₃**. Solid lines represent the best fit for the generalized Debye model.

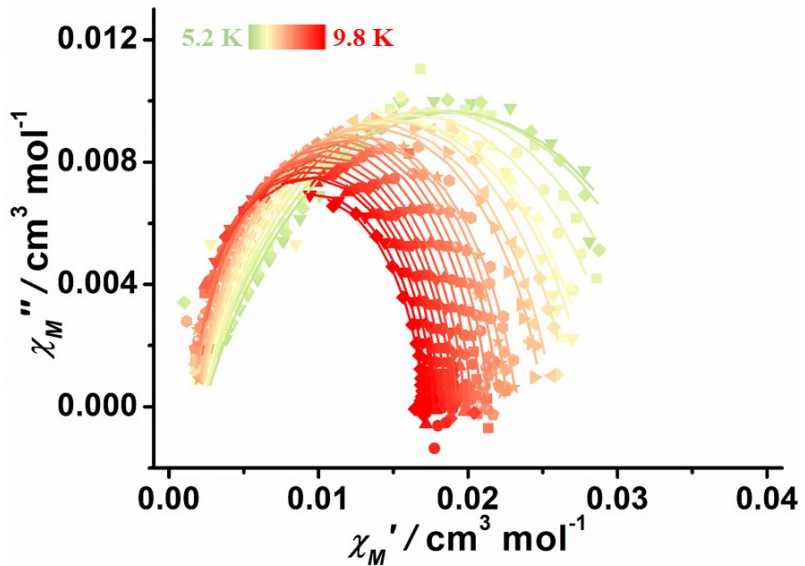


Figure S23. Cole-Cole plots for the ac susceptibilities under zero dc field for **2-NO₃@Zn**. Solid lines represent the best fit for the generalized Debye model.

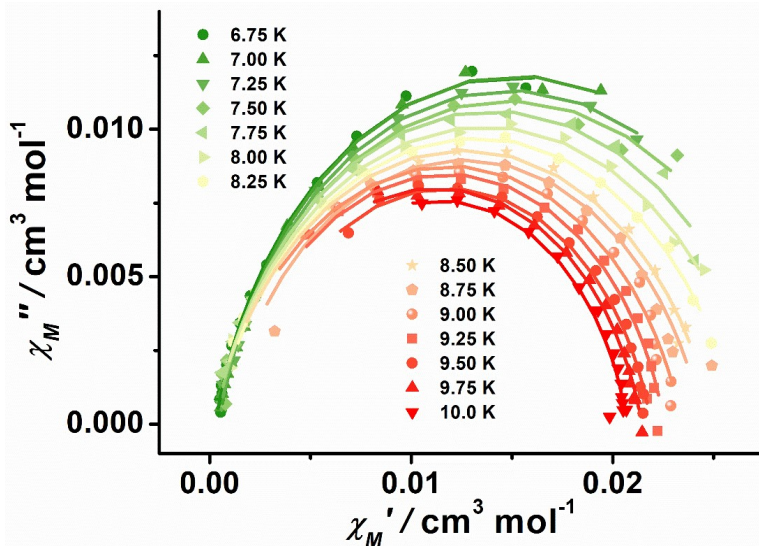


Figure S24. Cole-Cole plots for the ac susceptibilities under 1000 Oe dc field for **2-NO₃@Zn**. Solid lines represent the best fit for the generalized Debye model.

Table S5. Parameters obtained by fitting the Cole-Cole plot under zero dc field for **1-BPh₄**.

| T / K | χ_s | χ_T | τ | a |
|-------|----------|----------|---------|------|
| 3 | 0.32 | 0.69 | 0.02289 | 0.31 |
| 3.5 | 0.27 | 0.59 | 0.02003 | 0.32 |
| 4 | 0.24 | 0.52 | 0.02015 | 0.31 |
| 4.5 | 0.23 | 0.46 | 0.01959 | 0.25 |
| 4.8 | 0.20 | 0.44 | 0.01757 | 0.31 |
| 5 | 0.20 | 0.41 | 0.01767 | 0.23 |
| 5.2 | 0.19 | 0.40 | 0.01521 | 0.20 |
| 5.4 | 0.19 | 0.39 | 0.01338 | 0.15 |
| 5.6 | 0.19 | 0.37 | 0.01114 | 0.09 |
| 5.8 | 0.18 | 0.36 | 0.00865 | 0.06 |

Table S6. Parameters obtained by fitting the Cole-Cole plot under 200 Oe dc field for **1-BPh₄**.

| T / K | χ_s | χ_T | τ | a |
|-------|----------|----------|---------|------|
| 3.8 | 0.15 | 0.71 | 3.11175 | 0.25 |
| 4 | 0.14 | 0.56 | 1.29383 | 0.17 |
| 4.2 | 0.14 | 0.52 | 0.76138 | 0.15 |
| 4.4 | 0.13 | 0.49 | 0.45309 | 0.11 |
| 4.6 | 0.13 | 0.46 | 0.27496 | 0.09 |
| 4.8 | 0.12 | 0.44 | 0.17117 | 0.09 |
| 5.0 | 0.11 | 0.42 | 0.10622 | 0.09 |
| 5.2 | 0.11 | 0.40 | 0.0644 | 0.08 |
| 5.4 | 0.10 | 0.38 | 0.0399 | 0.05 |
| 5.6 | 0.094 | 0.37 | 0.02492 | 0.06 |
| 5.8 | 0.089 | 0.36 | 0.01588 | 0.05 |
| 6.0 | 0.087 | 0.35 | 0.01041 | 0.03 |
| 6.2 | 0.080 | 0.34 | 0.00686 | 0.03 |

Table S7. Parameters obtained by fitting the Cole-Cole plot under zero dc field for **1-BPh₄@Zn**.

| T / K | χ_s | χ_T | τ | a |
|-------|----------|----------|---------|------|
| 4.4 | 0.0068 | 0.076 | 0.41774 | 0.38 |
| 4.6 | 0.0073 | 0.067 | 0.23153 | 0.30 |
| 4.8 | 0.0076 | 0.061 | 0.14165 | 0.23 |
| 5.0 | 0.0068 | 0.057 | 0.08875 | 0.19 |
| 5.2 | 0.0061 | 0.054 | 0.056 | 0.16 |
| 5.4 | 0.0061 | 0.051 | 0.03645 | 0.12 |
| 5.6 | 0.0065 | 0.049 | 0.02467 | 0.09 |
| 5.8 | 0.0068 | 0.047 | 0.01651 | 0.07 |
| 6.0 | 0.0058 | 0.045 | 0.01088 | 0.06 |
| 6.2 | 0.0067 | 0.044 | 0.00772 | 0.04 |

Table S8. Parameters obtained by fitting the Cole-Cole plot under 200 Oe dc field for **1-BPh₄@Zn**.

| T / K | χ_s | χ_T | τ | a |
|-------|----------|----------|---------|------|
| 3.5 | 0.0069 | 0.093 | 5.66722 | 0.21 |
| 3.8 | 0.0064 | 0.077 | 2.14289 | 0.16 |
| 4.0 | 0.0058 | 0.072 | 1.29762 | 0.15 |
| 4.2 | 0.0057 | 0.066 | 0.77692 | 0.11 |
| 4.4 | 0.0055 | 0.062 | 0.47585 | 0.09 |
| 4.6 | 0.0049 | 0.059 | 0.29971 | 0.08 |
| 4.8 | 0.0048 | 0.056 | 0.1847 | 0.07 |
| 5.0 | 0.0046 | 0.055 | 0.11856 | 0.07 |
| 5.2 | 0.0042 | 0.052 | 0.0745 | 0.06 |
| 5.4 | 0.0032 | 0.050 | 0.04484 | 0.07 |
| 5.6 | 0.0041 | 0.048 | 0.02982 | 0.05 |
| 5.8 | 0.0042 | 0.046 | 0.01888 | 0.03 |
| 6.0 | 0.0047 | 0.045 | 0.01284 | 0.04 |
| 6.2 | 0.0010 | 0.043 | 0.00769 | 0.04 |

Table S9. Parameters obtained by fitting the Cole-Cole plot under zero dc field for **2-NO₃**.

| T / K | χ_s | χ_T | τ | a |
|-------|----------|----------|---------|------|
| 2.0 | 0.56 | 1.30 | 0.01673 | 0.42 |
| 2.3 | 0.48 | 1.14 | 0.01644 | 0.42 |
| 2.6 | 0.43 | 1.01 | 0.01609 | 0.42 |
| 2.9 | 0.39 | 0.91 | 0.016 | 0.42 |
| 3.2 | 0.35 | 0.83 | 0.01595 | 0.42 |
| 3.5 | 0.32 | 0.76 | 0.01557 | 0.42 |
| 3.8 | 0.30 | 0.70 | 0.01556 | 0.42 |
| 4.1 | 0.28 | 0.65 | 0.01564 | 0.42 |
| 4.4 | 0.26 | 0.61 | 0.0159 | 0.41 |
| 4.7 | 0.25 | 0.57 | 0.01572 | 0.41 |
| 5.0 | 0.23 | 0.54 | 0.01535 | 0.41 |
| 5.3 | 0.23 | 0.51 | 0.01634 | 0.40 |
| 5.6 | 0.22 | 0.48 | 0.01662 | 0.39 |
| 5.9 | 0.21 | 0.46 | 0.01726 | 0.38 |
| 6.1 | 0.20 | 0.43 | 0.01749 | 0.36 |
| 6.4 | 0.20 | 0.41 | 0.01795 | 0.34 |
| 6.7 | 0.19 | 0.40 | 0.01718 | 0.35 |
| 7.0 | 0.19 | 0.38 | 0.01814 | 0.29 |
| 7.3 | 0.19 | 0.36 | 0.01751 | 0.25 |
| 7.6 | 0.18 | 0.35 | 0.01615 | 0.21 |
| 7.9 | 0.18 | 0.34 | 0.01422 | 0.16 |
| 8.2 | 0.17 | 0.32 | 0.01146 | 0.13 |
| 8.5 | 0.16 | 0.31 | 0.0091 | 0.10 |
| 8.8 | 0.16 | 0.30 | 0.00699 | 0.08 |
| 9.1 | 0.16 | 0.29 | 0.0052 | 0.06 |
| 9.4 | 0.14 | 0.28 | 0.0038 | 0.05 |
| 9.7 | 0.13 | 0.27 | 0.00303 | 0.04 |

Table S10. Parameters obtained by fitting the Cole-Cole plot under zero dc field for **2-NO₃@Zn**.

| T / K | χ_s | χ_T | τ_1 | a_1 |
|-------|----------|----------|----------|-------|
| 5.2 | 0.0023 | 0.035 | 1.43305 | 0.33 |
| 5.4 | 0.0021 | 0.035 | 1.2276 | 0.32 |
| 5.6 | 0.0023 | 0.033 | 0.96422 | 0.27 |
| 5.8 | 0.0022 | 0.031 | 0.72923 | 0.24 |
| 6 | 0.0022 | 0.029 | 0.57377 | 0.21 |
| 6.2 | 0.0020 | 0.028 | 0.47297 | 0.21 |
| 6.4 | 0.0021 | 0.027 | 0.39316 | 0.17 |
| 6.6 | 0.0020 | 0.026 | 0.31153 | 0.16 |
| 6.8 | 0.0018 | 0.025 | 0.25176 | 0.15 |
| 7.2 | 0.0015 | 0.023 | 0.15504 | 0.13 |
| 7.4 | 0.0017 | 0.023 | 0.12252 | 0.11 |
| 7.6 | 0.0015 | 0.022 | 0.0963 | 0.10 |

| | | | | |
|-----|---------|-------|---------|------|
| 7.8 | 0.0016 | 0.021 | 0.07366 | 0.08 |
| 8 | 0.0016 | 0.021 | 0.05682 | 0.08 |
| 8.2 | 0.0018 | 0.020 | 0.04347 | 0.06 |
| 8.4 | 0.0012 | 0.020 | 0.03176 | 0.08 |
| 8.6 | 0.0012 | 0.019 | 0.02392 | 0.07 |
| 8.8 | 0.0011 | 0.019 | 0.01825 | 0.08 |
| 9.0 | 0.00087 | 0.019 | 0.01358 | 0.09 |
| 9.2 | 0.0012 | 0.018 | 0.01067 | 0.07 |
| 9.4 | 0.0012 | 0.018 | 0.00818 | 0.06 |
| 9.6 | 0.0020 | 0.017 | 0.00673 | 0.06 |
| 9.8 | 0.0018 | 0.017 | 0.00514 | 0.07 |

Table S11. Parameters obtained by fitting the Cole-Cole plot under 1000 Oe dc field for **2-NO₃@Zn**.

| T / K | χ_s | χ_T | τ | a |
|-------|----------|----------|---------|------|
| 6.75 | ~0 | 0.030 | 0.6334 | 0.14 |
| 7 | ~0 | 0.030 | 0.46498 | 0.14 |
| 7.25 | ~0 | 0.029 | 0.34678 | 0.15 |
| 7.5 | ~0 | 0.029 | 0.25992 | 0.18 |
| 7.75 | ~0 | 0.028 | 0.17752 | 0.17 |
| 8 | ~0 | 0.027 | 0.12383 | 0.18 |
| 8.25 | ~0 | 0.026 | 0.08405 | 0.18 |
| 8.5 | ~0 | 0.025 | 0.05698 | 0.18 |
| 8.75 | ~0 | 0.024 | 0.04235 | 0.17 |
| 9 | ~0 | 0.023 | 0.0274 | 0.17 |
| 9.25 | ~0 | 0.023 | 0.01965 | 0.15 |
| 9.5 | 0.0017 | 0.022 | 0.01467 | 0.15 |
| 9.75 | 0.0011 | 0.021 | 0.00993 | 0.15 |
| 10 | 0.0021 | 0.021 | 0.00765 | 0.13 |

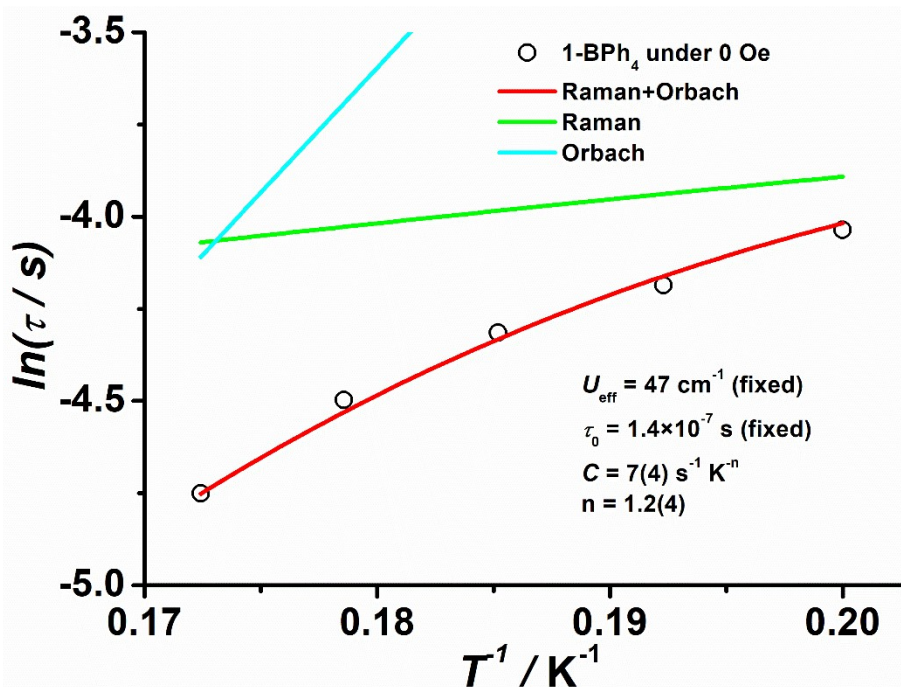


Figure S25. Temperature dependence of the magnetization relaxation rates under 0 Oe dc field for 1-BPh₄. The red line represents the best fit to a combination of Raman and Orbach processes, while the green and cyan lines represent the Raman and Orbach contributions to the magnetic relaxation, respectively.

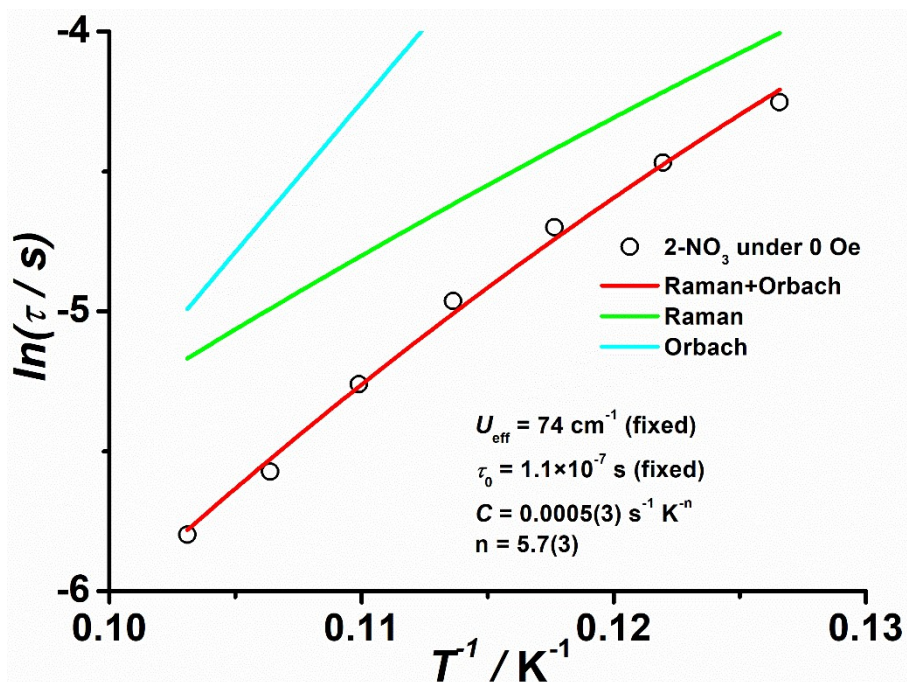


Figure S26. Temperature dependence of the magnetization relaxation rates under 0 Oe dc field for 2-NO₃. The red line represents the best fit to a combination of Raman and Orbach processes, while the green and cyan lines represent the Raman and Orbach contributions to the magnetic relaxation, respectively.

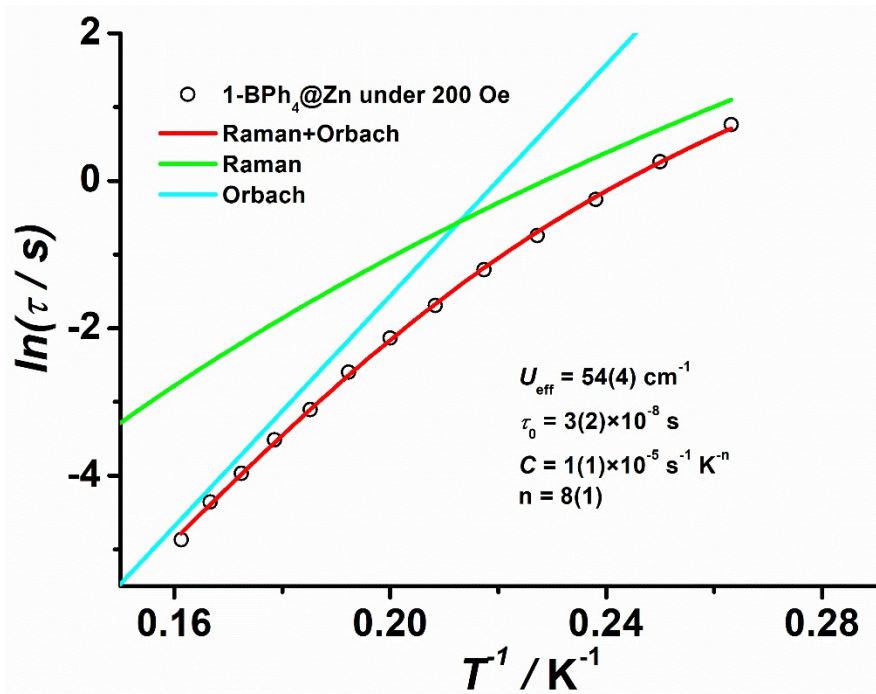


Figure S27. Temperature dependence of the magnetization relaxation rates under 200 Oe dc field for 2-NO₃@Zn. The red line represents the best fit to a combination of Raman and Orbach processes, while the green and cyan lines represent the Raman and Orbach contributions to the magnetic relaxation, respectively.

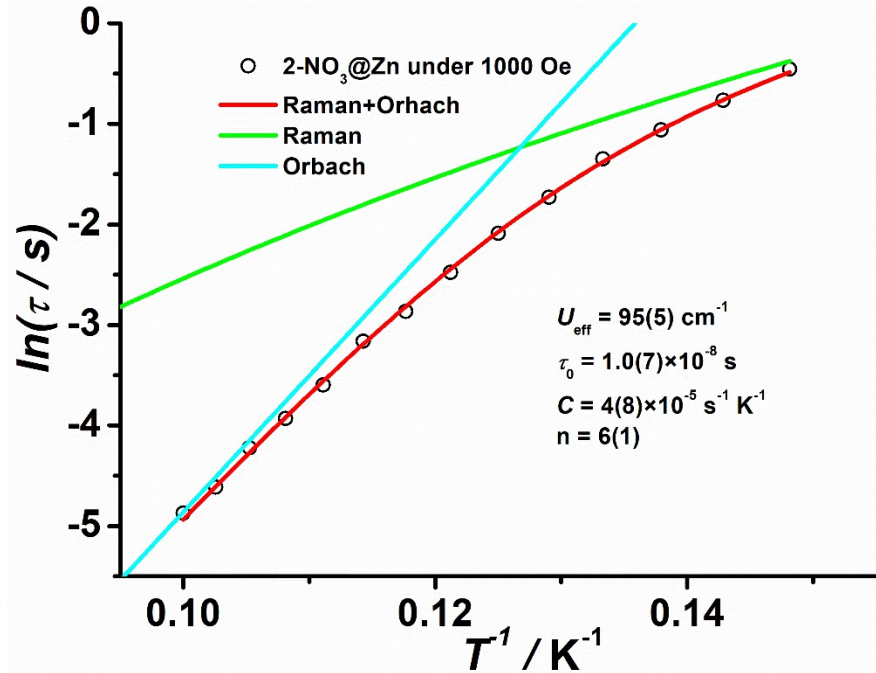


Figure S28. Temperature dependence of the magnetization relaxation rates under 1000 Oe dc field for 2-NO₃@Zn. The red line represents the best fit to a combination of Raman and Orbach processes, while the green and cyan lines represent the Raman and Orbach contributions to the magnetic relaxation, respectively.

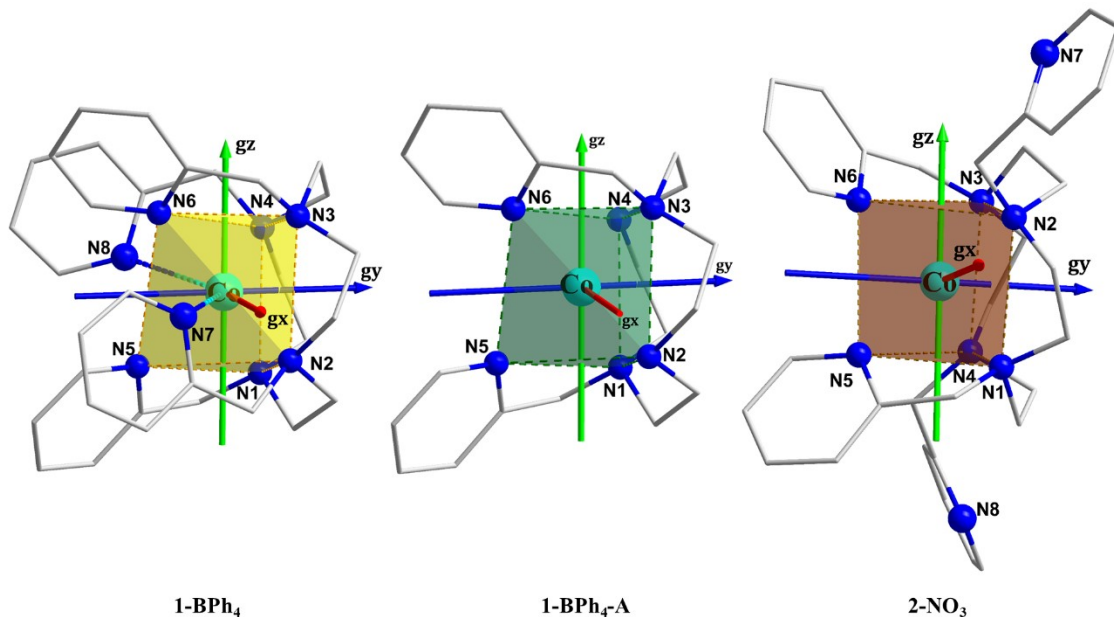


Figure S29. Orientations of the local magnetic axes (red: g_x ; blue: g_y ; green: g_z) on the Co(II) ions in all complexes in their ground spin-orbit states (results from NEVPT2 with the program Orca 5.0.4).

Table S12. Calculated ZFS parameters $D(E)$ (cm^{-1}) and ground \mathbf{g} (g_x , g_y , g_z) tensors of complexes **1-BPh₄**, **1-BPh₄-A** and **2-NO₃** using NEVPT2 with the program Orca 5.0.4.

| Complexes | NEVPT2 | | | | |
|----------------------------|------------------|------------------|-------|-------|-------|
| | D_{cal} | E_{cal} | g_x | g_y | g_z |
| 1-BPh₄ | -26.3 | -1.0 | 2.155 | 2.191 | 2.492 |
| 1-BPh₄-A | -32.7 | -0.7 | 2.148 | 2.178 | 2.555 |
| 2-NO₃ | -50.8 | -0.7 | 2.111 | 2.138 | 2.725 |

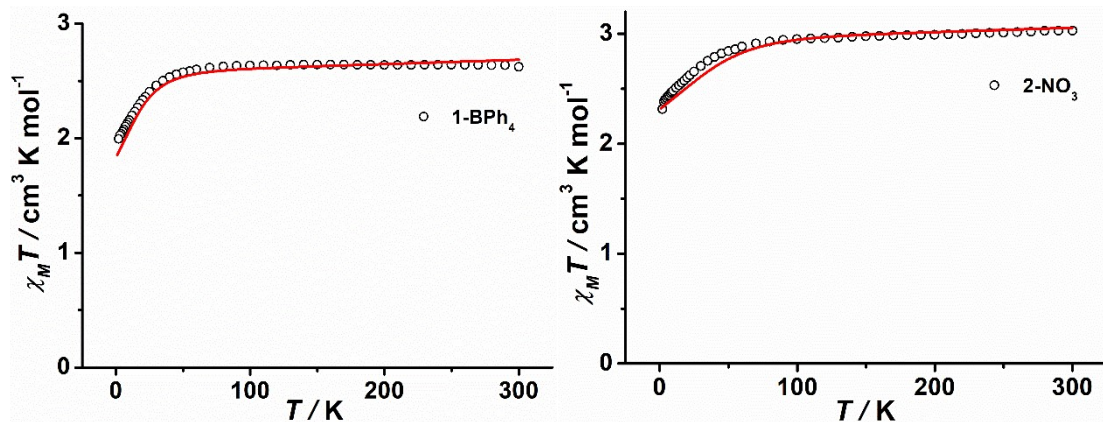


Figure S30. Calculated (red solid line) data of magnetic susceptibilities of **1-BPh₄** and **2-NO₃** using NEVPT2 with the program Orca 5.0.4.

Table S13. Selected important contributions of the spin-free excited states (with relative energy cm⁻¹) to D values (cm⁻¹) for complexes **1-BPh₄** and **2-NO₃** using NEVPT2 with the program Orca 5.0.4.

| Complexes | State No. | Mult | Energy | Contribution |
|----------------------------|-----------|------|--------|--------------|
| 1-BPh₄ | 1 | 4 | 1704.8 | -44.5 |
| | 3 | 4 | 4454.1 | 9.6 |
| | 2 | 4 | 4164.4 | 3.4 |
| 1-BPh₄-A | 1 | 4 | 1473.6 | -50.6 |
| | 3 | 4 | 4574.5 | 9.3 |
| | 4 | 4 | 6662.2 | 3.8 |
| 2-NO₃ | 1 | 4 | 1022.5 | -68.2 |
| | 3 | 4 | 5078.2 | 8.4 |
| | 4 | 4 | 6825.3 | 4.0 |

Table S14. Relative energies (cm⁻¹) of ligand field one-electron states (in the basis of d-AOs) of complexes **1-BPh₄** and **2-NO₃** from AILFT analysis using NEVPT2 with the program Orca 5.0.4.

| Complexes | No. | LF one-electron state | Energy |
|----------------------------|-----|---|--------|
| 1-BPh₄ | 0 | - 0.70 d _{x2-y2} + 0.69 d _{z2} | 0.0 |
| | 1 | - 0.61 d _{z2} - 0.59 d _{x2-y2} + 0.52 d _{yz} | 566.7 |
| | 2 | 0.97 d _{xy} - 0.22 d _{xz} | 1566.8 |
| | 3 | - 0.85 d _{yz} - 0.38 d _{z2} - 0.34 d _{x2-y2} | 5362.3 |
| | 4 | - 0.95 d _{xz} - 0.22 d _{xy} | 7734.8 |
| 1-BPh₄-A | 0 | 0.91 d _{x2-y2} - 0.31 d _{z2} + 0.23 d _{yz} | 0.0 |
| | 1 | 0.81 d _{z2} + 0.54 d _{yz} + 0.16 d _{x2-y2} | 465.2 |
| | 2 | 0.98 d _{xy} + 0.16 d _{xz} | 908.5 |
| | 3 | - 0.81 d _{yz} + 0.45 d _{z2} + 0.36 d _{x2-y2} | 4908.5 |
| | 4 | 0.97 d _{xz} - 0.17 d _{xy} + 0.16 d _{z2} | 7602.5 |
| 2-NO₃ | 0 | 0.91 d _{z2} + 0.42 d _{yz} | 0.0 |
| | 1 | 0.95 d _{x2-y2} + 0.27 d _{yz} | 271.8 |
| | 2 | 0.98 d _{xy} + 0.17 d _{xz} | 984.6 |
| | 3 | - 0.86 d _{yz} + 0.40 d _{z2} + 0.31 d _{x2-y2} | 5676.9 |
| | 4 | - 0.99 d _{xz} + 0.17 d _{xy} | 8240.0 |

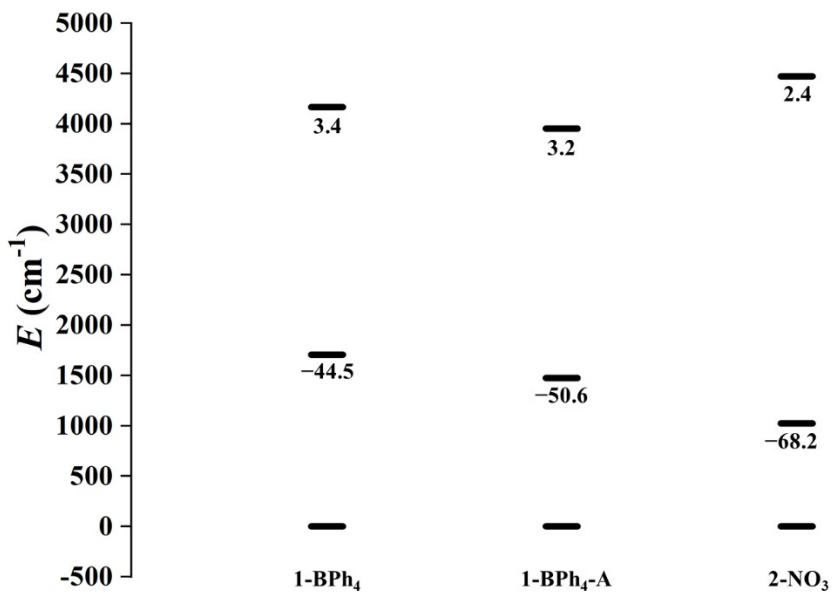


Figure S31. Energy gap between the ground, first and second excited quartet states computed for **1-BPh₄**, **1-BPh₄-A** and **2-NO₃**. The numerical value below each state gives its contribution to the *D* value (in cm^{-1}).

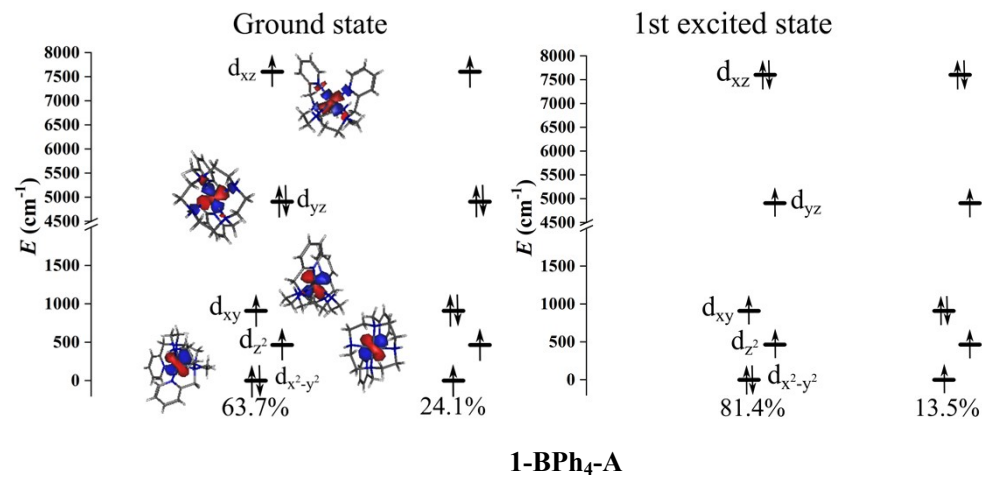


Figure S32. Orbital energies computed for the ground and first excited state of model complex **1-BPh₄-A** using NEVPT2 with the program Orca 5.0.4. Values in percent indicate the contribution to configuration mixing.